Solid-state phase equilibria in the Er-Nd-Fe ternary system at 1073 K

M. Saidi, K. Nouri, S. Walha, L. Bessais, M. Jemmali

Version of Record: https://www.sciencedirect.com/science/article/pii/S0925838820321186
Manuscript_c1aa991faba61ae2a9521ce9f3110540

Solid-state phase equilibria in the Er-Nd-Fe ternary system at 1073 K

M. Saidi,[1,2] K. Nouri,[1,2] S. Walha,[2] L. Bessais *,[1] and M. Jemmali[2,3]

[1] *Univ Paris Est Creteil, CNRS, ICMPE, UMR 7182, F-94320 Thiais, France.*

[2] *University of Sfax, Faculty of Science, LSME, BP1171-3018 Sfax, Tunisia.*

[3] *Department of Chemistry, College of Science and Arts, Ar-rass, Qassim University, PO Box 53, Buraydah Postcode 51921, Saudi Arabia.*

* Author to whom correspondence should be addressed; electronic mail: bessais @icmpe.cnrs.fr

Abstract

The solid state phase equilibria in the ternary Er-Nd-Fe system at 1073 K in all the composition ranges were investigated using the experimental results of the X-ray powder diffraction analysis (XRD) as well as those obtained from the Scanning electron microscopy (SEM) equipped with Energy dispersive spectroscopy (EDS). The binary systems ErFe, ErNd and Nd-Fe were investigated prior to the study of the ternary one. Six binary compounds were identified to exist at this isothermal section at 1073 K namely: $ErFe_2$ ($Fd\bar{3}m$-$MgCu_2$ structure type), $ErFe_3$ ($R\bar{3}m$-$PuNi_3$ structure type), Er_6Fe_{23} (Fm-3m-Th_6Mn_{23} structure type), Er_2Fe_{17} ($P6_3/mmc$-Th_2Ni_{17} structure type), Nd_2Fe_{17} ($R\bar{3}m$-Th_2Zn_{17} structure type), and δ-NdEr ($R\bar{3}m$-Sm structure type). No new ternary compounds were found in all investigated ternary alloy samples. The phase relations are governed by seven three-phase regions, sixteen two-phase regions and nine single-phase regions, as well as a small liquid area in the Nd-rich region. At 1073 K, we have observed that the highest solubility of Nd in $ErFe_2$ is about 16.6 at. % Nd, while the $Er_{1-x}Nd_xFe_3$ solid solution based on binary $ErFe_3$ extends up to 7.5 at. % Nd. The XRD and the SEM/EDS analyses show that there is no miscibility of Nd in Er_6Fe_{23}. The pair of the binary compounds Er_2Fe_{17} and Nd_2Fe_{17} extend through the ternary system parallel to the Nd-Er edge. The maximum homogeneity range of the $Er_{2-x}Nd_xFe_{17}$ solid solution reaches 5.3 at. % Nd, while that of the $Nd_{2-x}Er_xFe_{17}$ solid solution is about 1.6 at. % Er. In the Er-Nd binary system, the maximum solid solubility of Nd in Er is about 38.4 at. % Nd, and the solubility limit of Er in Nd is about 29.8 at. % Er.

PACS numbers:

I. INTRODUCTION

With the industrial development across the world and the continuous improvement of the people's living standard, more research has been made to explore new magnetic intermetallic materials with a potential to be utilized in efficient technologies such as magnetic refrigeration. This technology can replace the conventional refrigeration based on the compressionexpansion of greenhouse gases such as CFC (ChloroFluoroCarbons) and HCFC (Hydro-ChloroFluoroCarbons) [1]. In addition, magnetic refrigerators are much more compactly built due to the fact of employing magnetic materials such as refrigeration media. This technology presents many advantages like ecological cleanliness; reliability; compactness; and low noise [2–4].

Over several decades, intermetallic compounds formed by alloying rare-earth (R) and transition metal (M) have been extensively investigated [5]. Indeed, these compounds have resulted in a significant amount of research due to their outstanding magnetic and magnetocaloric properties. The magnetic properties of these intermetallic compounds are governed by the combination of the complementary characteristics of 3d itinerant magnetism of transition metal atoms and that of 4f localized magnetism of the rare earth atoms [6, 7]. The Fe-rich R_2Fe_{17} intermetallic compound has particularly known a great success in the field of refrigeration thanks to its magnetic and magnetocaloric properties shown around room temperature such as Y_2Fe_{17}, Pr_2Fe_{17} [8, 9], Tb_2Fe_{17} [10] Gd_2Fe_{17} [11] and Er_2Fe_{17} [12, 13].

The study of phase equilibria is of paramount importance for providing a basis for searching new magnetic materials and improving their performance. Moreover, the assessment of the ternary phase diagrams is valuable for improving the synthetic route of high purity samples, especially those not yet magnetically characterized. The phase diagrams of R-Fe-M systems are sufficiently rich in ternary and binary compounds, which have attracted broad interest with respect to their interesting crystal chemistry and varying physical properties. In recent years, these ternary systems R-Fe-M have been intensively studied for (R= Nd, Sm, Gd, Er and Y; M = Cu, Cr, Al, Co, Ni, Ge and Ga) [14–20], in the interest of reaching a better understanding of the properties of the intermetallic materials.

Additionally, some research on the ternary systems consisting of two rare earth elements and a transition metal has already been done. In this context, in the R-Nd-Fe and Er-Nd-M ternary systems, the phase relationships have already been established for (R = Pr, Sm,

Ga and Sb) [21–24], and (M = Mn and Co) [25, 26] respectively. However, no investigation on the phase diagram of the ErNd-Fe ternary system has been investigated so far. The scope of this paper represents a continuation of previously conducted studies on ternary systems based on iron and two rare-earth elements (R). The purpose of this paper is to systematically investigate the phase equilibria of the ErNd-Fe ternary system at 1073 K in order to determine the phases relation and their stability and to explore intermetallic compounds with important magnetic and magnetocaloric properties.

II. EXPERIMENTAL DETAILS

For the study of the interaction in the Er-Nd-Fe ternary system, 50 binary and ternary samples have been synthesized, whose compositions are plotted in the Gibbs triangles in Figure 1. The starting materials were used in the form of pieces of high purity elements: Er (99.9 wt.%), Nd (99.9 wt.%) and Fe (99.9 wt.%). The polycrystalline samples (each one weighing 0.5 g) were prepared by melting the calculated amounts of the elements in an arc furnace under high purified argon atmosphere and in a water-cooling copper crucible with an inconsumable tungsten electrode. The resulting button was re-melted three times and turned over after each melting to promote good homogeneity. After the synthesis, the buttons were wrapped into tantalum sheets and encapsulated into quartz ampoules. Tantalum foils were used to prevent direct contact of the samples with silica during annealing and to avoid a possible contamination with silicon. Silica glass tubes were then sealed and annealed at 1073 K for seven days in a resistance furnace to improve the atomic diffusion kinetics and good crystallinity of the samples. After the annealing process, the ampoules were immediately quenched in cold water to preserve the equilibrium state and to retain the high-temperature microstructure of the samples. The weight loss, which was controlled at all stages of the synthesis, did not exceed 1 % of the total mass. Thereafter, each prepared ingot was divided into two pieces. One piece was ground into powder in a mortar for X-ray diffraction analysis, while the other was used for Scanning electron microscopy.

The X-ray phase measurement (XRD) analysis was the main method for isothermal section construction. It was made using a Brucker diffractometer (Brucker, Thiais, France) with copper CuKα radiation ($\lambda_{K\alpha 1}$= 1.5406 Å) in order to identify the present phases as well as to examine the crystallographic structure of the prepared samples. The data were

collected at room temperature over a 2θ ranging from 20° to 80°, with a step size of 0.015° and counting rate of 13.5 s per Scanning step. Indexing of the obtained diffraction data of the ternary samples was performed by the comparison between the observed powder patterns and those calculated using the Powdercell software package [27]. The data treatment was carried on using the Fullprof computer code [28], based on the Rietveld method [29, 30], in the assumption of Thompson-Cox-Hastings line profile [31, 32].

For the microstructural examination and quantitative phase analyses, samples were mounted onto a sample-support (Metal conductor) in the polisher. Grinding was carried out on water-cooled SiC abrasive paper using finer and finer grits as well as polishing slurry. This was followed by polishing using diamond abrasive paper to make the surface shine. The metallographic study and EDS analysis were performed to check the results of the X-ray diffraction analysis using a Merlin Scanning electron microscopy (SEM) with a Silicon Drift Detector (SDD)-X-Max 50 equipped with Energy dispersive X-ray spectroscopy (EDS). Eventually, this characterization technique was utilized to study the chemical composition and the morphology of phases in the samples.

III. BINARY SYSTEMS

The isothermal section of phase diagram is an important basis for materials research and application. The boundaries of the phase equilibria of Er-Nd-Fe system involve three binary systems: Nd-Fe, Er-Fe and Er-Nd, which have been widely investigated.

The Nd-Er system, which was studied by both G. F. Kobzenko *et al.* [33] and K.A. Gschneidner *et al.* [34], is considered to be the simplest system because only one binary compound was found in it which is δ-NdEr. Investigations on the Nd-Er binary system reported that metals Nd and Er can substitute each other and form solid solutions.

The phase equilibra in the Nd-Fe binary system have been extensively studied in previous years. This binary system was constructed for the first time in 1965 by V. E Terekhova *et al.* [35]. Later on, several investigations on the study of the same binary system have been made by A. E. Ray [36], G. Schneider *et al.* [37] and F. Faudot *et al.* [38]. In the NdFe binary system, only one intermetallic compound was identified, namely Nd_2Fe_{17}. This system was subsequently re-investigated by F.J.G. Landgraf *et al.* [39]. They proved the presence of a new stable phase Nd_5Fe_{17} and showed a revised phase diagram of the Nd-

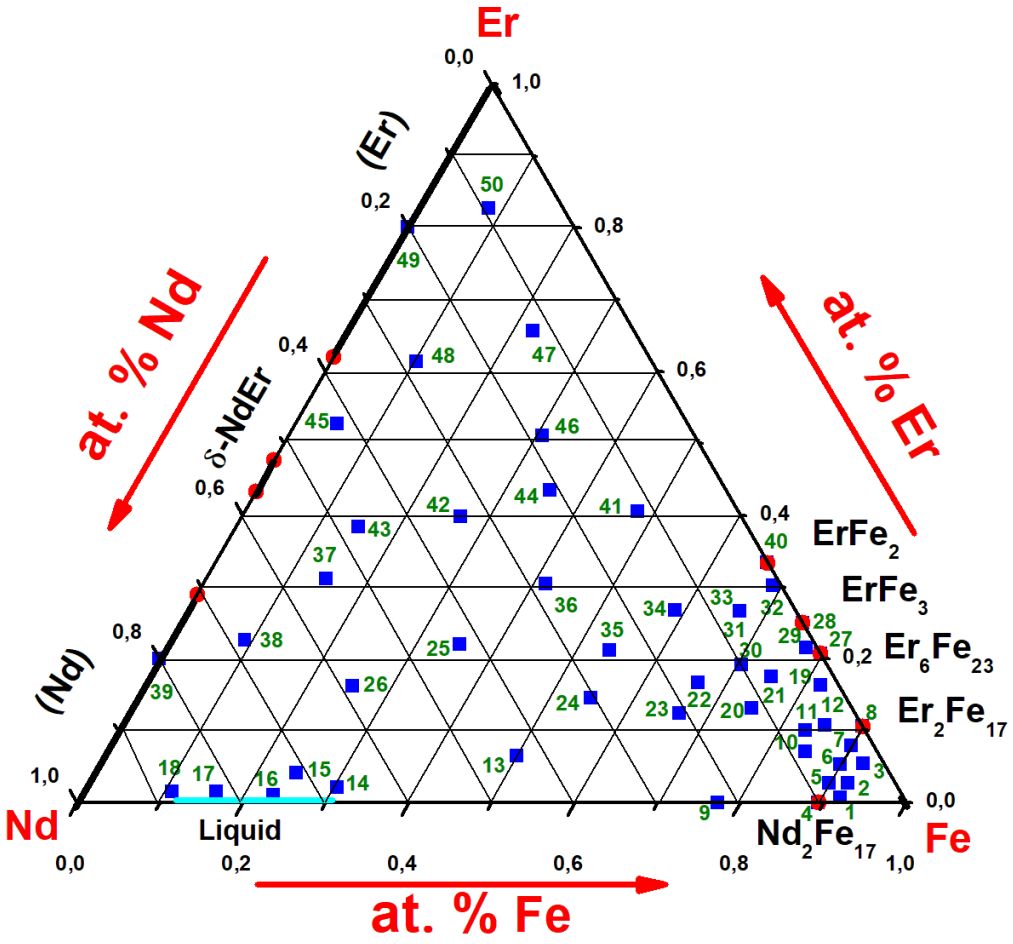

FIG. 1: Prepared compositions of the Er-Nd-Fe samples.

Fe system. Lately, R. Marazza *et al.* [40] performed a recent assessment of this binary system. Two intermediate binary phases were confirmed to exist: Nd_2Fe_{17} (rhombohedral; Th_2Zn_{17} structure type) and Nd_5Fe_{17}(rhombohedral; Nd_5Fe_{17} type-structure) which formed peritectically at 1481 K and 1025 K, respectively. According to this result, Nd_5Fe_{17} phase is only stable at T $<$ 1025 K. In the study of the Nd-Pt-Fe ternary phase diagram at 1173 K, the same result was then verified by Xu Chengfu *et al.* [41]. They demonstrated that no diffraction peaks of Nd_5Fe_{17} were found through careful analysis of the XRD patterns of the Nd_5Fe_{17} compound, which proved that Nd_5Fe_{17} had completely decomposed into Nd_2Fe_{17} and Nd.

The entire binary phase diagram Er-Fe has been discussed by many scholars. K. H. J.

Buschow and A. S. van der Goot [42] studied the phase relations, crystal structures, and magnetic properties of the intermetallic compounds in the ErFe system using X-ray powder diffraction (XRD), metallographic methods, and differential thermal analysis (DTA). Four binary compounds $ErFe_2$, $ErFe_3$, Er_6Fe_{23} and Er_2Fe_{17} were identified. Three among them, $ErFe_3$, Er_6Fe_{23} and Er_2Fe_{17} decompose at 1618 K, 1603 K, and 1628 K, respectively. The fourth compound $ErFe_2$ melts congruently at 1633 K. Two eutectic and three peritectic transformations in this system were also reported [42]. Later, A. Meyer [43] investigated the phase diagram of the ErFe system by means of Differential thermal analysis, Scanning electron microscopy and X-ray diffraction. The phase relations determined by A. Meyer [43] were consistent with those of K. H. J. Buschow and A. S. van der Goot [42]. Nevertheless, the invariant reaction temperatures were different. In comparison with the results of A. Meyer [43], all the melting points of the compounds were lower than those found by K. H. J. Buschow and A. S. van der Goot [42] (by up to about 70 K). Later on, V.E. Kolesnikov *et al.* [44] also determined the binary system Er-Fe, and proved the presence of a fifth compound which is $ErFe_5$. Recently, G. J. Zhou *et al.* [45] assessed thermodynamically the ErFe system on the basis of the earlier work of K. H. J. Buschow and A. S. van der Goot [42], A. Meyer [43], and V.E. Kolesnikov *et al.* [44], and announced finally the existence of four intermetallic compounds $ErFe_2$ ($MgCu_2$-structure type), $ErFe_3$ ($PuNi_3$-structure type), Er_6Fe_{23} (Th_6Mn_{23}-structure type), and Er_2Fe_{17} (Th_2Ni_{17}-structure type) in the Er-Fe system. Detailed crystallographic data for the Er-Fe and Nd-Fe intermediate compounds are listed in Table I.

IV. RESULTS AND DISCUSSION

A. Solid solubility

In this paper, we have studied the binary systems Nd-Er, Nd-Fe and Er-Fe at 1073 K to verify the binary compounds before the phase analysis in the ternary system.

In the Nd-Er binary section, one intermetallic binary compound was found, namely δ-NdEr, which is in line with the previous results [34]. Furthermore, metals Nd and Er substitute each other to form single-phase regions. Therefore, at 1073 K the maximum solid solubility of Nd in Er is measured to be about 38.4 at. % Nd, while the maximum solid

TABLE I: Crystallographic data of intermatallic binary compounds in Er-Nd-Fe ternary system at 1073 K.

Phase Composition	Structure type	Space group	Lattice parameters (Å)		References
			a	c	
$ErFe_2$	$MgCu_2$	$Fd\bar{3}m$	7.272(2)	-	[46]
$ErFe_3$	$PuNi_3$	$R\bar{3}m$	5.080(2)	24.398(8)	[46]
Er_6Fe_{23}	Th_6Mn_{23}	$Fm\bar{3}m$	11.959(2)	-	[46]
Er_2Fe_{17}	Th_2Ni_{17}	$P6_3/mmc$	8.415(3)	8.323(4)	[46]
Nd_2Fe_{17}	Th_2Zn_{17}	$R\bar{3}m$	8.557(1)	12.443(5)	[47]
Nd_5Fe_{17}	Nd_5Fe_{17}	$P6_3/mcm$	20.207(3)	12.341(6)	[48]
δ-NdEr	Sm	$R\bar{3}m$	3.611(4)	26.221(3)	[49]

solubility of Er in Nd is determined to be about 29.8 at. % Er. Moreover, the intermediate binary phase δ-NdEr covers an homogeneity range from 52.4 at. % Nd to 56.7 at. % Nd. The limits of this homogeneity domains are in agreement with those previously reported in ref [34].

In the NdFe binary system, the Nd_5Fe_{17} binary compound was found to be stable at a low temperature phase. Therefore, the present result confirmed the previous results of our team [17] and show that Nd_5Fe_{17} cannot exist stably at 1073 K, and should not be presented in the Nd-Fe-Er isothermal section. Thus, only the existence of the binary compound Nd_2Fe_{17} was confirmed in the NdFe section.

The boundary binary system ErFe studied in this paper depicted the existence of four binary compounds, Er_2Fe_{17} (Th_2Ni_{17}-structure type), Er_6Fe_{23} (Th_6Mn_{23}-structure type), $ErFe_2$ ($MgCu_2$-structure type) and $ErFe_3$ ($PuNi_3$-structure type). This result is consistent with the findings of the previous study mentioned in reference [45]. The binary phases in the Er-Fe system, exept Er_6Fe_{23}, extend into the ternary system forming solid solutions with changes in their unit cell parameters. The homogeneity ranges of these solid solutions were studied by means of X-ray powder diffraction, Scanning electron microscopy, and Energy dispersion spectroscopy techniques. The various concentrations of Er/Nd were chosen to delineate the limit of these extensions into the Er-Nd-Fe isothermal section and to verify the structure type.

The existence of the $Er_{1-x}Nd_xFe_2$ solid solution at 1073 K was revealed by the synthesis of several samples on the linear solid solubility and in the side regions. The analysis of the XRD and the SEM/EDS results of each sample allowed the delimitation of the $Er_{1-x}Nd_xFe_2$ solid solution. The extended solid solution based on the $ErFe_2$ cubic Laves C15 binary phase was found to cover the composition range from $ErFe_2$ to $Er_{0.5}Nd_{0.5}Fe_2$ with a structural stability ($MgCu_2$-structure type, $Fd\bar{3}m$ space group) over all the range homogeneity domain. The XRD pattern of the Er19-Nd44-Fe37 nominal composition (N° 25 in Figure 1), located in the two-phase region 4 of the ternary phase diagram, pointed out a solid state equilibrium between the limit of the solid solution $Er_{1-x}Nd_xFe_2$ (x = 0.5) and Er_xNd_{1-x} (x = 0.3) (Figure 2). The microstructure was examined by SEM and clearly showed the existence the following compositions: $Er_{1-x}Nd_xFe_2$ (x = 0.5) and Er_xNd_{1-x} (x = 0.3), as presented in Figure 3. The darker grey areas show the phase $Er_{0.3}Nd_{0.7}$ and the bright grey areas show the phase $Er_{0.5}Nd_{0.5}Fe_2$.

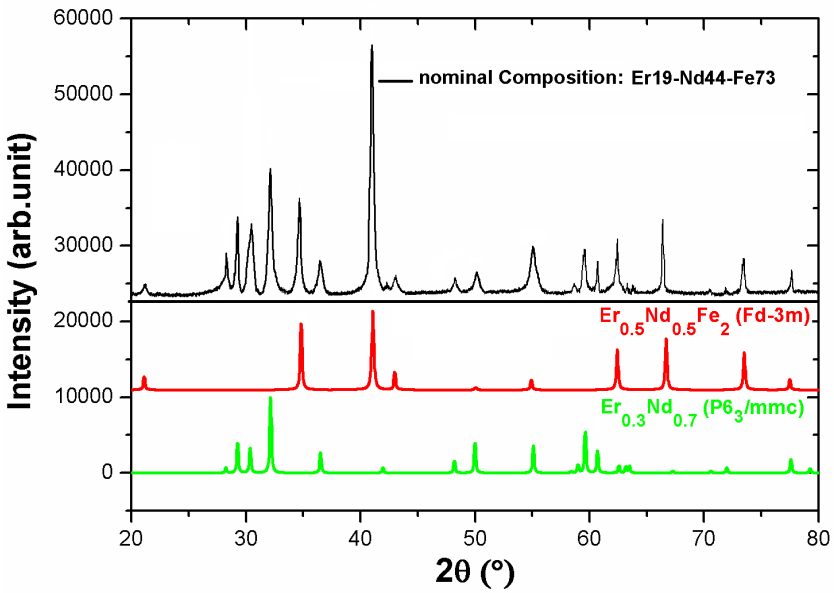

FIG. 2: Experimental XRD pattern of the Er19-Nd44-Fe37 nominal composition showing the equilibrium between $Er_{0.3}Nd_{0.7}$ and $Er_{0.5}Nd_{0.5}Fe_2$.

In order to further confirm the existence of the linear solid solubility, we also examined the experimental X-ray diffractogram (Figure 4) of the Er12-Nd22-Fe66 nominal composition (N°23 in Figure 1) located in the three-phase region C of the Er-Fe-Nd ternary system, which is indexed to three structure types, and shows the three-phase equilibrium between

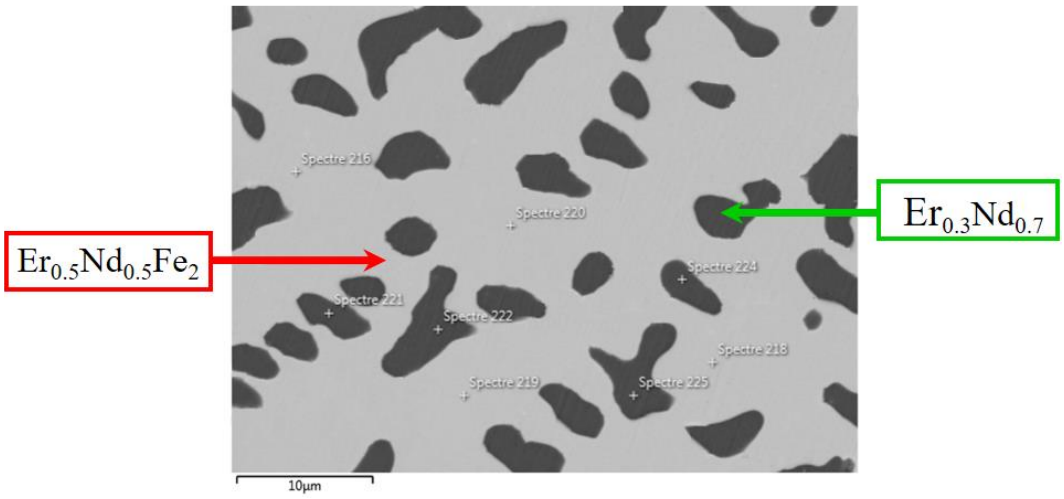

FIG. 3: Backscattered electron SEM image of the Er19-Nd44-Fe37.

the following phases: $Er_{1-x}Nd_xFe_2$ (x = 0.5) ($MgCu_2$-structure type) + Nd_2Fe_{17} (Th_2Zn_{17} -structure type) + Nd (Nd-structure type). The SEM micrograph image of the Er12-Nd22-Fe66 composition presented in Figure 5 shows the thermodynamic equilibrium between the upper limit of the $Er_{1-x}Nd_xFe_2$ solid solution which is $Er_{0.5}Nd_{0.5}Fe_2$ (bright grey phase), the Nd_2Fe_{17} binary phase (dark grey phase), and Nd (medium grey phase). The atomic radius of Nd (1.821 Å) is bigger than that of Er (1.757 Å). Therefore, the result obtained agree with Vegard's law. The unit cell parameters of the solid solutions increase when Er in solid solutions is substituted by Nd at 1073 K. The unit cell parameter of the $Er_{1-x}Nd_xFe_2$ ($0 \leq x \leq 0.5$) solid solution increase from about $a = 7.272(2)$ Å to $a = 7.285(3)$ Å, when x were changed from 0 to 0.5.

The stability of the $Er_{1-x}Nd_xFe_3$ solid solution was confirmed using both SEM-EDS and X-ray diffraction analysis. The synthesis of the Er21-Nd2-Fe77 nominal composition (N° 20 in Figure 1) in the three-phase region D of the Er-Fe-Nd ternary phase diagram revealed the limit of this solid solution. The X-ray powder diffraction pattern (Figure 6) as well as the microstructure (Figure 7) of the Er21-Nd2-Fe77 nominal composition, which was melted and heat-treated at 1073 K, clearly show a solid state equilibrium between the upper limit of the solid solution $Er_{1-x}Nd_xFe_3$ (x = 0.3), the upper limit of the solid solution $Er_{1-x}Nd_xFe_2$ (x = 0.5), and the Nd_2Fe_{17} binary phase. The SEM image, presented in Figure 7, indicates that the dark grey phase is identified as $Er_{1-x}Nd_xFe_2$ (x = 0.5), the medium grey one as Nd_2Fe_{17}, while the bright grey one as $Er_{1-x}Nd_xFe_3$ (x = 0.3). This result proves that the

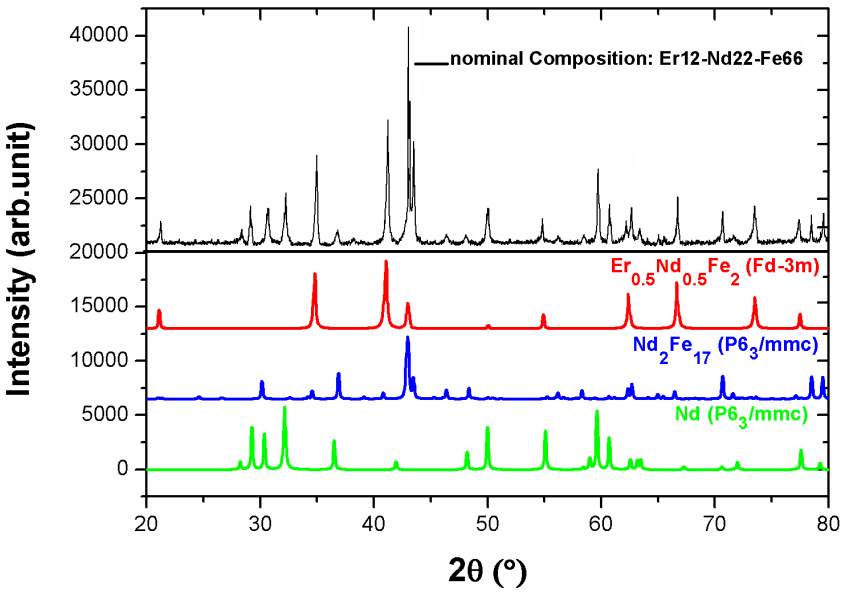

FIG. 4: XRD pattern of the Er12-Nd22-Fe66 nominal composition showing the two-phase equilibrium between $Er_{0.5}Nd_{0.5}Fe_2$, Nd_2Fe_{17} and Nd.

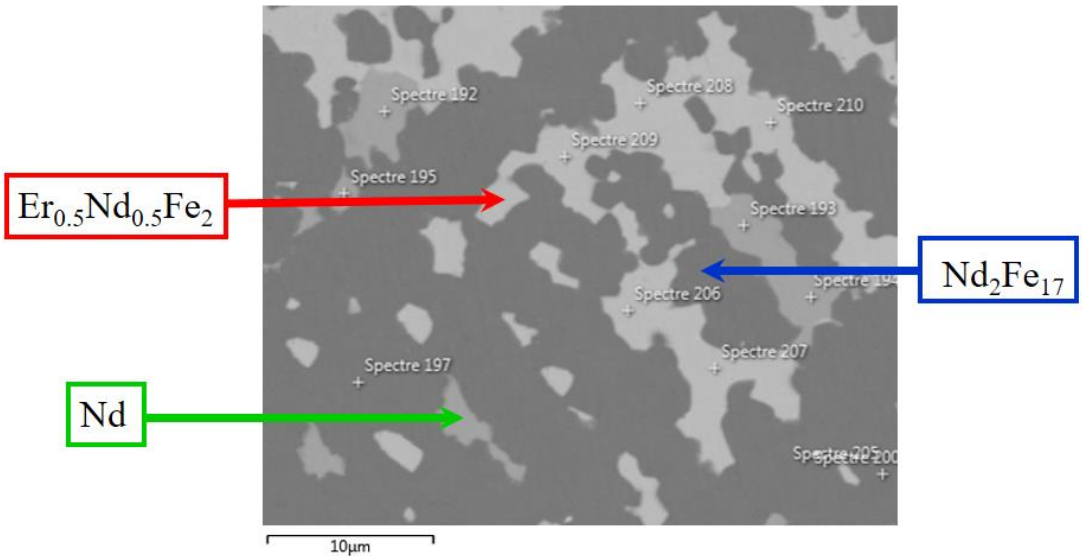

FIG. 5: Backscattered electron SEM image of the Er12-Nd22-Fe66 nominal composition.

solubility of Nd in the $Er_{1-x}Nd_xFe_3$ solid solution, which crystallizes in the rhombohedral type-structure with the $R\bar{3}m$ space group, reaches 7.5 at. % Nd at 1073 K. During the study of this homogeneity domain, the same type of structure of $PuNi_3$ was preserved.

Furthemore, the systematic studies of the phase equilibria in the Fe-rich region confirmed the solubility limit in which Nd dissolves in $ErFe_3$. The XRD pattern (Figure 8) for the

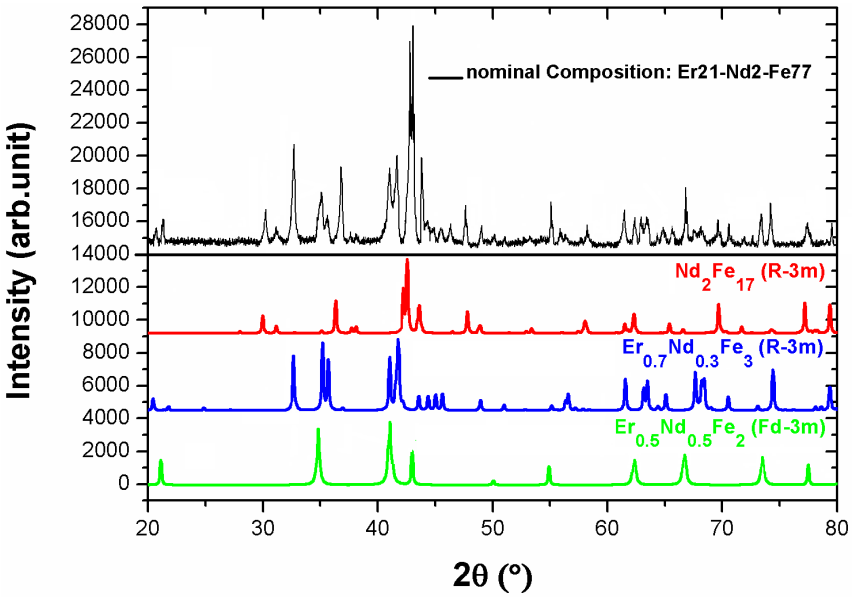

FIG. 6: XRD pattern of the Er21-Nd2-Fe77 nominal composition located in the $Er_{0.5}Nd_{0.5}Fe_2$ + $Er_{0.7}Nd_{0.3}Fe_3$ + Nd_2Fe_{17} three-phase region.

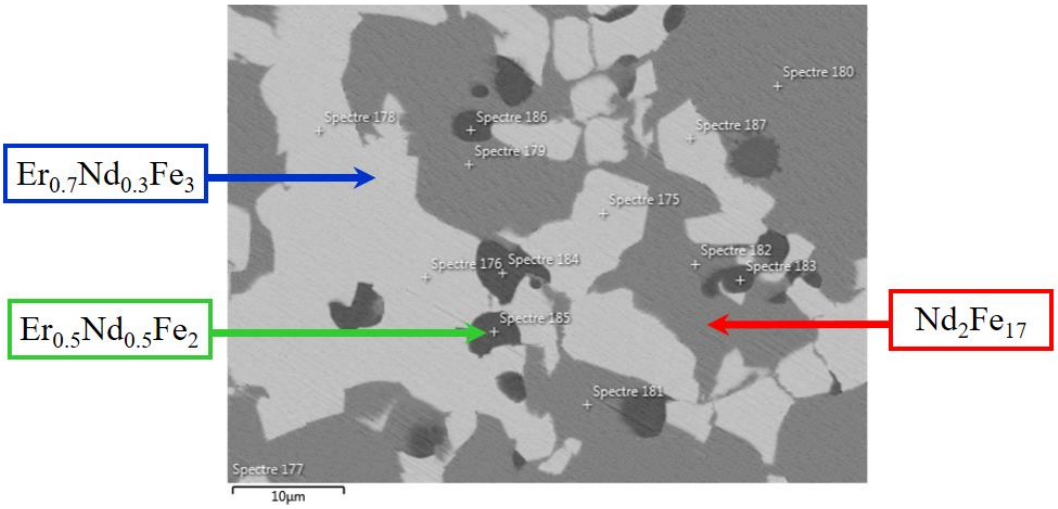

FIG. 7: Backscattered electron image of the Er21-Nd2-Fe77 nominal composition showing the three-phase equilibrium between $Er_{0.5}Nd_{0.5}Fe_2$, $Er_{0.7}Nd_{0.3}Fe_3$ and Nd_2Fe_{17}.

Er16-Nd81-Fe3 nominal composition (N°19 in Figure 1) prepared in the three-phase region E consists of the patterns of the upper limit of the solid solution $Er_{1-x}Nd_xFe_3$ (x = 0.3) ($PuNi_3$-structure type), the Er_2Fe_{17} binary phase (Th_2Ni_{17}-structure type), and the Er_6Fe_{23} binary phase (Th_6Mn_{23}-structure type). The SEM image micrograph presented in Figure 9

attests to the result of the X-ray pattern, and shows that the dark grey, medium grey, and bright grey areas had atomic compositions in agreement with $Er_{1-x}Nd_xFe_3$ (x = 0.3), Er_2Fe_{17}, and Er_6Fe_{23}, respectively. The refined unit cell parameters of the $Er_{1-x}Nd_xFe_3$ (x = 0.3) composition were obtained as follows : $a = 5.098(6)$ Å and $c = 24.422(3)$ Å.

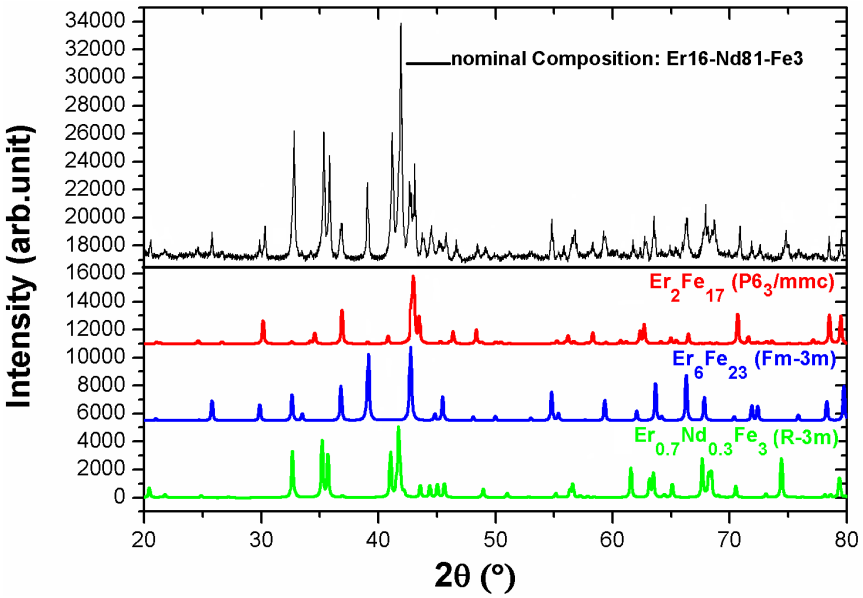

FIG. 8: XRD pattern of the Er16-Nd81-Fe3 nominal composition.

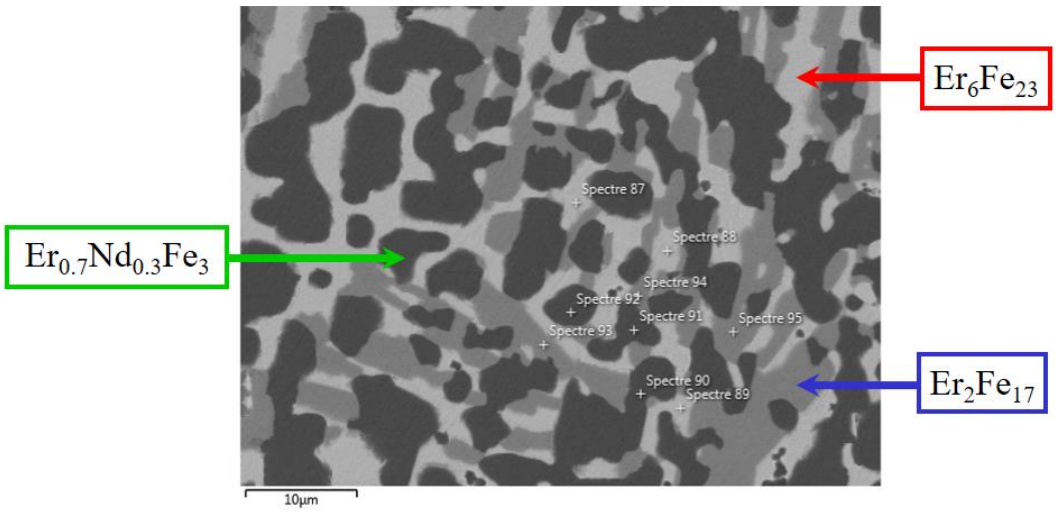

FIG. 9: Backscattered electron image of the Er16-Nd81-Fe3 nominal composition.

The R_2Fe_{17} compound was found to be crystallized in two polymorphic forms. Some only exhibit the rhombohedral Th_2Zn_{17} structure with $R\bar{3}m$ space group, if R is lighter than

gadolinium (for example Pr_2Fe_{17} [10] and Nd_2Fe_{17} [50]), while others exhibit the hexagonal Th_2Ni_{17} structure with $P6_3/mmc$ space group, if R is heavier than dysprosium (for example Ho_2Fe_{17} [51] and Er_2Fe_{17} [12]). In this paper, the Rietveld refinement of Er_2Fe_{17} (Figure 10) shows that it crystallizes in the hexagonal Th_2Ni_{17}-structure type with the unit cell parameters $a = 8.435(7)$ Å and $c = 8.281(8)$ Å. Whereas, the Rietveld analysis of Nd_2Fe_{17} presented in Figure 11, proves that this binary phase adopts the rhombohedral Th_2Zn_{17}-structure type with the unit cell parameters: a = 8.548(6) Å and c = 12.446(5) Å.

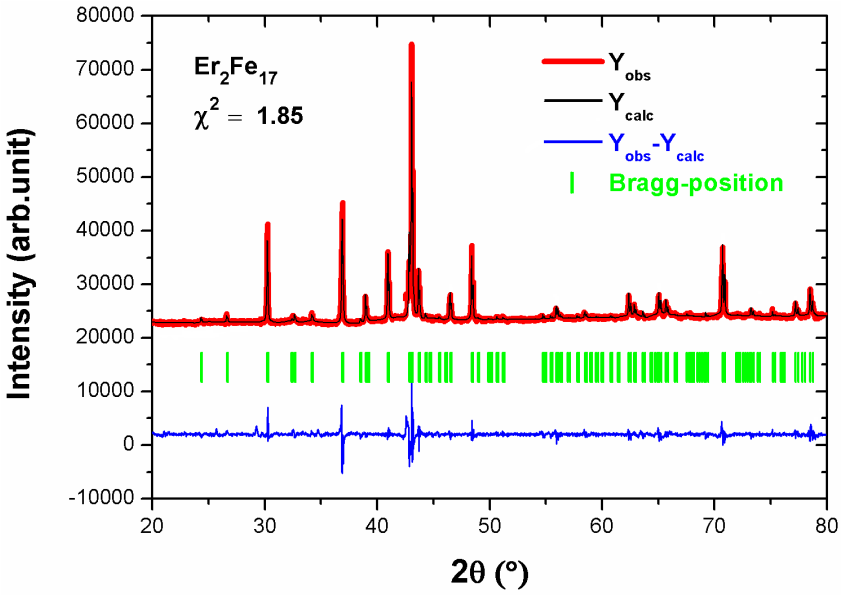

FIG. 10: Observed (dots) and calculated (solid line) XRD patterns of Er_2Fe_{17} annealed at 1073 K. Vertical bars represent the positions of the Bragg reflections.

According to our results at 1073 K, erbium and neodym are mutually soluble in each other in the 2/17 binary phase. In order to identify the $(Er/Nd)_2Fe_{17}$ solid solution at 1073 K, we synthesized several samples on this binary extension. The XRD patterns of the $Er_{2-x}Nd_xFe_{17}$ (x = 0, 0.5, 1, 1.5 and 2) compounds, shown in Figure 12, demonstrate the obtaining of pure single phases having the same hexagonal Th_2Ni_{17}-structure type for x = 0, 0.5 and 1, while the compound with x = 2 crystallizes in the rhombohedral Th_2Zn_{17}-structure type. However, the XRD pattern reveals that the sample with x = 1.5 can be indexed by both the rhombohedral Th_2Zn_{17}-type 2/17 phase and the hexagonal Th_2Ni_{17}-type 2/17 phase. In Figure 12, we illustrated the diffraction peaks of phase Er_2Fe_{17} with black stars and those of phase Nd_2Fe_{17} with red lozenges. We observed that the pair of binary compounds Er_2Fe_{17}

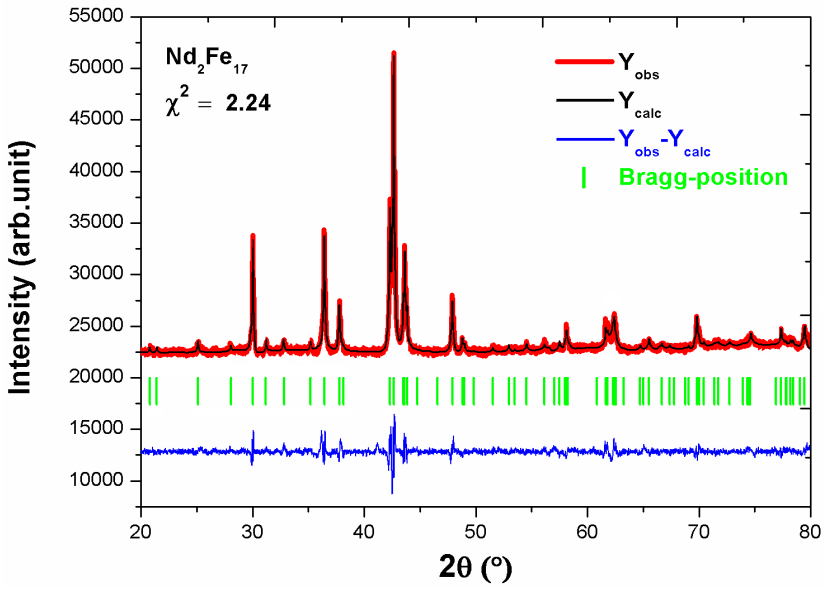

FIG. 11: Observed (dots) and calculated (solid line) XRD patterns of Nd_2Fe_{17} annealed at 1073 K. Vertical bars represent the positions of the Bragg reflections.

and Nd_2Fe_{17} extend through the ternary system parallel to the Er-Nd edge and form two solid solutions. The maximum solid solubility of Nd in the compound Er_2Fe_{17} was about 5.3 at. % Nd pointing to a wide range of Nd substituting Er in the $Er_{2-x}Nd_xFe_{17}$ solid solution from x = 0 to x = 1. Whereas, the $Nd_{2-x}Fe_xFe_{17}$ solid solution with the rhombohedral Th_2Zn_{17}-structure type covers the composition range between x = 0 and x = 0.3. The refined unit cell parameters of the $Er_{2-x}Nd_xFe_{17}$ (x = 1) composition are : $a = 8.451(2)$ Å and $c = 8.297(4)$ Å. While, the refined unit cell parameters of the $Nd_{2-x}Fe_xFe_{17}$ (x = 0.3) composition are : $a = 8.531(4)$ Å and $c = 12.429(3)$ Å.

The studied Er-Fe-Nd isothermal section in the whole concentration range in this paper has not been investigated so far. However, the investigated compounds $Nd_{2-x}Er_xFe_{17}$ (x = 0, 0.5, 1, 1.5 and 2) have already been studied by Y. G. Xiao *et al.* in order to determine the interesting effects of rare earths mixing on the structural and magnetic properties of the 2/17 rare earth-transition metal intermetallic compounds [52].

B. Phase equilibrium at 1073 K

Based on analyzing the results obtained from the X-ray diffraction technique with the aid of SEM/EDS analysis, we have determined the solid state phase equilibria of Er-Fe-Nd

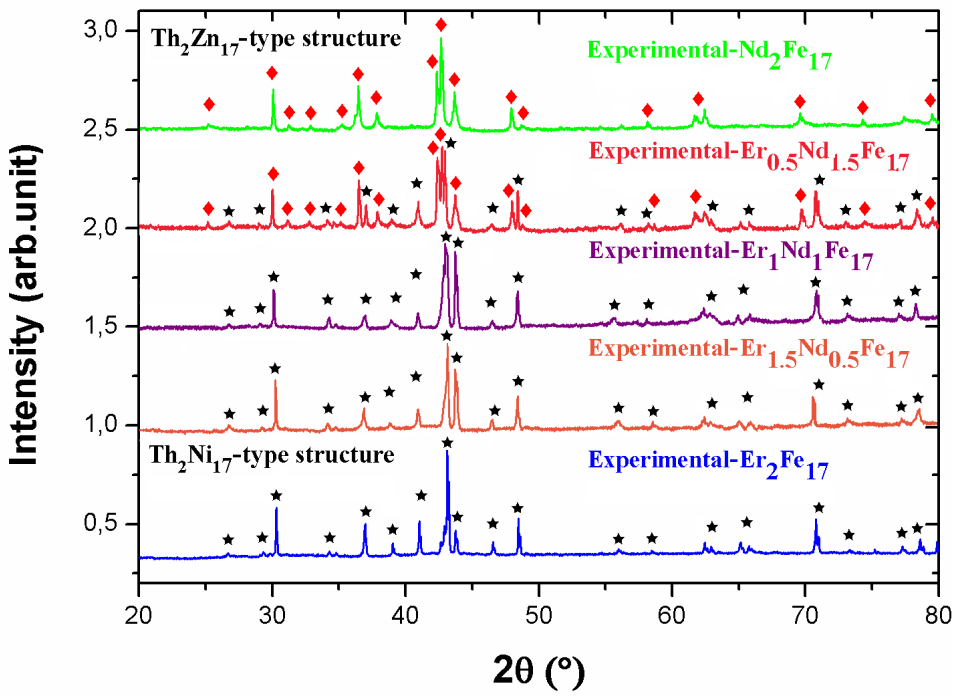

FIG. 12: XRD patterns of the $Er_{2-x}Nd_xFe_{17}$ (x = 0, 0.5, 1, 1.5 and 2) samples.

system. The isothermal section of the phase diagram of Er-Fe-Nd system is shown herewith in Figure 13. In this paper, we have confirmed the existence of six binary compounds stable at 1073 K. At this temperature, the existence of all binary compounds of the Er-Fe system: $ErFe_2$, $ErFe_3$, Er_6Fe_{23} and Er_2Fe_{17} have been confirmed. At 1073 K, the Nd-Fe and Nd-Er systems are characterized by the formation of the binay compounds Nd_2Fe_{17} and δ-NdEr respectively. No ternary compounds were observed in the isothermal section. The binary compounds $ErFe_2$, $ErFe_3$ and Er_2Fe_{17} dissolve certain amounts of the third element Nd, and form extended homogeneity regions. The extended regions of solid solubility of each single phase in the ternary phase diagram were clearly identified. The $ErFe_3$ compound crystallizes in the rhombohedral $PuNi_3$-structure type and has a quite large extension in the ternary diagram. The maximum solid solubility of Nd in the $ErFe_3$ was found to be about 7.5 at. % Nd, leading to the chemical formula $Er_{0.7}Nd_{0.3}Fe_3$. In addition, we pointed out that the Laves phase with a stoichiometry AB_2 is stable for the solid solution $Er_{1-x}Nd_xFe_2$ ($MgCu_2$-structure type) which covers the composition range from 0 to 16.6 at. % Nd. Moreover, the maximum homogeneity range of $Er_{2-x}Nd_xFe_{17}$ is about 5.3 at. % Nd, while that of $Nd_{2-x}Er_xFe_{17}$ is about 1.6 at. % Er. In the Nd-Er system, Nd and Er atoms can substitute

each other and form solid solutions because their atomic radii are close. At 1073 K, the maximum solid solubility of Er in Nd and Nd in Er is about 29.8 at. % Er and 38.4 at. % Nd, respectively. The intermediate binary phase δ-NdEr has a broad homogeneity range extending from about 52.4 at. % Nd to 56.7 at. % Nd.

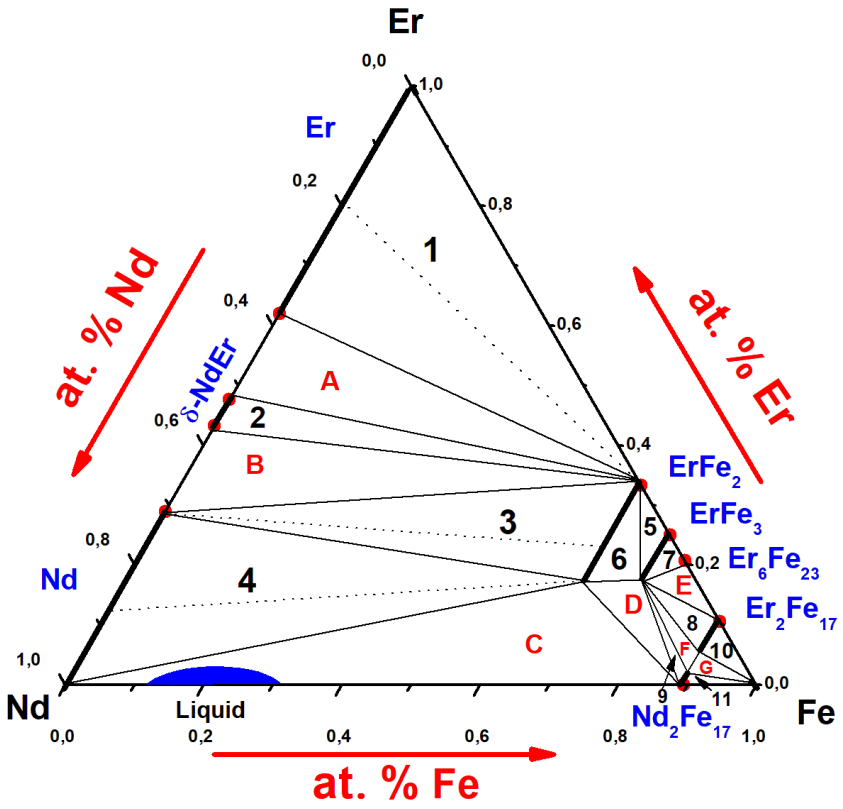

FIG. 13: The isothermal section of the Er-Nd-Fe ternary system at 1073 K.

The Er-Fe-Nd isothermal section of 1073 K possesses seven three-phase regions, sixteen two-phase regions, and nine single-phase regions. The XRD patterns of some representative samples located in some two-phase regions and three-phase regions are given in Figure 14. Based on the analysis of the XRD pattern shown in Figure 14.a, we have confirmed the existence of the two phases $ErFe_2$ and δ-NdEr in the sample with the atomic proportion of Er 40 %, Nd 34 % and Fe 26 % (N° 42 in Figure 1) located in the two-phase region 2.

Moreover, the equilibrated phases Er_2Fe_{17} + $ErFe_3$ (two-phase region 5) were defined from the analysis of the X-ray diffraction pattern (Figure 14.b) of the sample with the Er30-Nd2-Fe68 nominal composition (N° 32 in Figure 1).

Figure 14.c also illustrates the XRD pattern of the sample with the nominal composition Er19-Nd11-Fe70 (N°30 in Figure 1) prepared in the two-phase region 6. We could observe that the upper limit of the solid solutions $Er_{1-x}Nd_xFe_3$ (x = 0.3) and $Er_{1-x}Nd_xFe_2$ (x = 0.5) are confirmed in this equilibrated sample.

In addition, the XRD pattern presented in Figure 14.d, clearly indicates the existence of three phases Er_2Fe_{17}, $Er_{0.7}Nd_{0.3}Fe_3$, and Nd_2Fe_{17} in the equilibrated sample with the atomic proportion of Er 10 %, Nd 7 % and Fe 83 % (N° 11 in Figure 1) located in the three-phase region F.

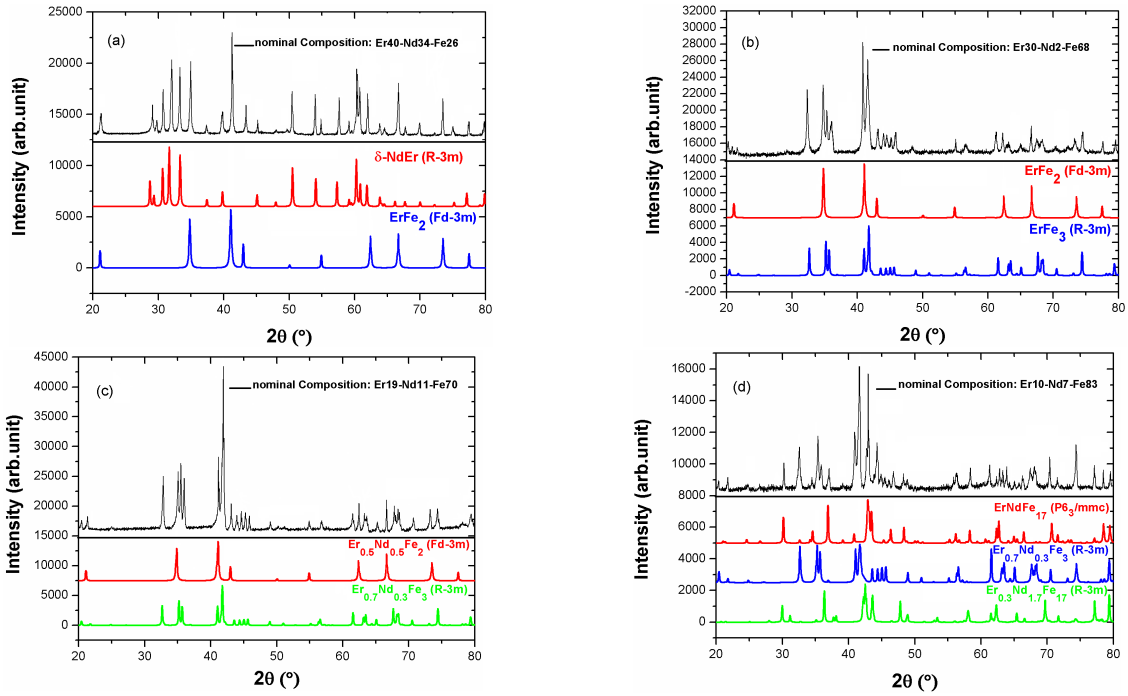

FIG. 14: The XRD pattern of the equilibrated samples: (a) Er40-Nd34-Fe26, (b) Er30-Nd2-Fe68, (c) Er19-Nd11-Fe70 and (d) Er10-Nd7-Fe83.

It is noteworthy that we have found in the binary Nd-Fe system a small liquid phase in the Nd-rich side in the range varying between 69.2 at. % Nd and 87.3 at. % Nd. The existence of the liquid area was proven by the fact that the two samples with nominal compositions Er2-Nd75-Fe23 (N°16 in Figure 1) and Er2-Nd82-Fe16 (N°17 in Figure 1) prepared respectively in the three-phase region C, were indeed found in a liquid state in the tantalum sheet after annealing for one week at 1073 K. Moreover, the XRD patterns of the three nominal compositions located in the three-phase region C surrounding this liquid composition show a solid state equilibrium between $ErFe_2$ and Nd. These three nominal

compositions are the following: Er3-Nd67-Fe30 (N°14 in Figure 1), Er6-Nd70-Fe24 (N°15 in Figure 1), and Er3-Nd87-Fe10 (N°18 in Figure 1). The details of the measured compositions by EDS with their numbers presented in Figure 1 in both two and three phase regions of the Er-Nd-Fe ternary system, are respectively listed as follows in Table II and III.

V. CONCLUSIONS

A series of Er-Nd-Fe alloys was designed to construct the 1073 K isothermal section of the Er-Nd-Fe system in the whole compositional range based on examination by a combination of X-ray powder diffraction (XRD) and Scanning electron microscope (SEM) equipped with Energy dispersive X-ray spectrometer (EDS). Some conclusions were drawn and given as follows:

(i) Nine single-phase regions, sixteen two-phase regions, seven three-phase regions and a small liquid area were identified to exist at this isothermal section at 1073 K.

(ii) The phase diagram of Er-Nd-Fe system at this temperature is characterized by the formation of six binary stable phases $ErFe_2$ ($MgCu_2$-structure type), $ErFe_3$ ($PuNi_3$-structure type), Er_6Fe_{23} (Th_6Mn_{23}-structure type), Er_2Fe_{17} (Th_2Ni_{17}-structure type), Nd_2Fe_{17} (Th_2Zn_{17}-structure type) and δ-NdEr (Sm-structure type). Among them, only four binary compound extended into the ternary system at constant iron composition due to the substitution of Er by Nd. The addition of Nd in the Er-Fe system did not stabilize the Th_6Mn_{23} structure type.

(iii) Based on X-ray powder diffraction and metallographic phase analyses, we have observed that the maximum solid solubility of Nd in $ErFe_2$ is below 16.6 at. % Nd. While, the binary $ErFe_3$ compound is found to dissolve up to 7.5 at. % Nd. Furthermore, at 1073 K, the $Er_{2-x}Nd_xFe_{17}$ solid solution adopts the hexagonal Th_2Ni_{17}-structure type and extends from x = 0 to x = 1, while the $Nd_{2-x}Fe_xFe_{17}$ solid solution with the rhombohedral Th_2Zn_{17}-structure type has a broad solubility ranging from x = 0 to x = 0.3.

(iv) To conclude, the study of the phase relationships in the Er-Nd-Fe ternary system at 1073 K is very interesting. This is because the construction of this phase diagram provides important information relating to the particularities of phase relations, the solubility limit and the stability of the rare earth-iron intermetallic compounds which exibit attractive magnetic and magnetocaloric properties.

TABLE II: Phase compositions of the two-phase regions in the Er-Nd-Fe ternary system at 1073 K.

Phase regions	No	Nominal compositions	Phases	EDS results (at.%)		
				Er	Nd	Fe
1	46	Er51-Nd18-Fe31	$ErFe_2$	33.1	0.0	66.9
			$Er_{0.62}Nd_{0.38}$	61.6	38.4	0.0
2	42	Er40-Nd34-Fe26	$ErFe_2$	33.5	0.0	66.5
			δ-NdEr	43.3	56.7	0.0
3	36	Er30-Nd28-Fe42	$ErFe_2$	33.2	0.0	66.8
			$Er_{0.3}Nd_{0.7}$	29.6	70.4	0.0
4	25	Er19-Nd44-Fe37	$Er_{0.5}Nd_{0.5}Fe_2$	16.7	16.6	66.7
			$Er_{0.3}Nd_{0.7}$	29.8	70.8	0.0
5	32	Er30-Nd2-Fe68	$ErFe_2$	33.4	0.0	66.6
			$ErFe_3$	25.1	0.0	74.9
6	30	Er19-Nd11-Fe70	$Er_{0.5}Nd_{0.5}Fe_2$	16.9	16.8	66.3
			$Er_{0.7}Nd_{0.3}Fe_3$	17.6	7.5	74.9
7	29	Er21-Nd3-Fe76	$ErFe_3$	24.8	0.0	75.2
			Er_6Fe_{23}	20.6	0.0	79.4
8	18	Er12-Nd4-Fe84	$ErNdFe_{17}$	5.6	5.4	89
			$Er_{0.7}Nd_{0.3}Fe_3$	17.4	7.6	74.9
9	10	Er7-Nd8-Fe85	$Er_{0.3}Nd_{1.7}Fe_{17}$	1.7	9.2	89.1
			$Er_{0.7}Nd_{0.3}Fe_3$	17.5	7.8	74.7
10	3	Er5-Nd3-Fe92	$ErNdFe_{17}$	24.8	0.0	75.2
			αFe	0.2	0.0	99.8
11	1	Er2-Nd7-Fe91	$Er_{0.3}Nd_{1.7}Fe_{17}$	1.8	9.1	89.1
			αFe	0.0	0.0	100

TABLE III: Phase compositions of the three-phase regions in the isothermal section of Er-Nd-Fe ternary system at 1073 K.

Phase regions	No	Nominal compositions	Phases	EDS results (at.%)		
				Er	Nd	Fe
A	41	Er40-Nd12-Fe48	$ErFe_2$	33.3	0.0	66.6
			$Er_{0.62}Nd_{0.38}$	61.1	38.9	0.0
			δ-NdEr	47.6	52.4	0.0
B	37	Er34-Nd42-Fe24	$ErFe_2$	33.7	0.0	66.3
			$Er_{0.3}Nd_{0.7}$	29.4	70.6	0.0
			δ-NdEr	43.4	56.6	0.0
C	23	Er12-Nd22-Fe66	Nd_2Fe_{17}	0.0	10.6	89.4
			$Er_{0.5}Nd_{0.5}Fe_2$	16.5	16.6	67.1
			Nd	0.0	100	0.0
D	20	Er21-Nd2-Fe77	Nd_2Fe_{17}	0.0	10.3	89.7
			$Er_{0.7}Nd_{0.3}Fe_3$	17.5	7.7	74.8
			$Er_{0.5}Nd_{0.5}Fe_2$	16.8	16.7	66.5
E	19	Er16-Nd81-Fe3	Er_6Fe_{23}	20.5	0.0	79.5
			$Er_{0.7}Nd_{0.3}Fe_3$	17.7	7.5	74.8
			Er_2Fe_{17}	10.7	0.0	89.3
F	11	Er10-Nd7-Fe83	$Er_{0.3}Nd_{1.7}Fe_{17}$	1.8	9.2	89
			$ErNdFe_{17}$	5.7	5.3	89
			$Er_{0.7}Nd_{0.3}Fe_3$	17.6	7.4	75
G	2	Er6-Nd2-Fe92	$ErNdFe_{17}$	5.4	5.5	89.1
			αFe	0.1	0.0	99.9
			$Er_{0.3}Nd_{1.7}Fe_{17}$	1.7	9.3	89

VI. ACKNOWLEDGMENTS

This work was mainly supported by the CNRS, the Tunisian Ministry of Higher Education and Scientific Research and Technology (LAB MESLAB) (Tunisia-Sfax).

VII. REFERENCES

[1] K. A. Gschneidner Jr, V. K. Pecharsky, and A. O. Tsokol, Rep. Prog. Phys. **68** (2005) 1479.

[2] M. H. Phan, and S. C. Yu, J. Magn. Magn. Mater. **308** (2007) 325.

[3] A. Kitanovski, and P. W. Egolf, J. Magn. Magn. Mater. **321** (2009) 777.

[4] E Brück, J. Phys. D: Appl. Phys. **38** (2005) R381.

[5] K. H. J. Buschow, Rep. Prog. Phys. **54** (1991) 1123.

[6] K. H. J. Buschow, Rep. Prog. Phys. **40** (1977) 1179.

[7] J. Pospisil, J. P. Vejpravova, D. Niznansky, and V. Sechovsky, J. Magn. Magn. Mater. **310** (2007) 629.

[8] K. Mandal, A. Yan, P. Kershl, A. Handstein, O. Gutfleisch, and K. H. Muller, J. Phys. D. **37** (2004) 2628.

[9] R. Guetari, R. Bez, A. Belhadj, K. Zehani, A. Bezergheanu, N. Mliki, L. Bessais, and C. Cizmas, J. Alloys Compd. **588** (2014) 64.

[10] S. Charfeddine, K. Zehani, L. Bessais, and A. Korchef, J. Solid State Chem. **238** (2016) 15.

[11] M. Saidi, K. Nouri, S. Walha, A. Kabadou, M. Jemmali, and L. Bessais, J. Electron. Mater. **48** (2019) 2242.

[12] P. A. Alonso, P. Gorria, J. S. Marcos, J. L. Sánchez Llamazares, and J. A. Blanco, J. Phys. Condens. Matter. **25** (2013) 496010.

[13] D. M. Khedr, S. H. Aly, R. M. Shabara, and S. Yehia, J. Magn. Magn. Mater. **475** (2019) 436.

[14] M. Saidi, S. Walha, K. Nouri, A. Kabadou, M. Jemmali, and L. Bessais, J. Alloys Compd. **781** (2019) 159.

[15] M. Saidi, S. Walha, K. Nouri, A. Kabadou, L. Bessais, and M. Jemmali, J. Alloys Compd. **792** (2019) 87.

[16] K. Nouri, M. Jemmali, S. Walha, A. B. Salah, E. Dhahri, and L. Bessais, J. Alloys Compd. **719** (2017) 256.

[17] N. Bouchaala, M. Jemmali, K. Nouri, S.Walha, A. B. Salah, and L. Bessais, J. Phase Equilib. Diffus. **38** (2017) 561.

[18] K. Nouri, M. Jemmali, S. Walha,, K. Zehani, A. B. Salah, and L. Bessais, J. Alloys Compd. **661** (2016) 508.

[19] M. Jemmali, S. Walha, R. Hassen, and H. Noël, Asian J. Chem. **28** (2016) 1330.

[20] M. Jemmali, S. Walha, M. Pasturel, O. Tougait, R. Hassen, and H. Noël, J. Alloys Compd. **489** (2010) 421.

[21] T. Chen, C. Guo, C. Li, and Z. Du, Thermochim. Acta. **680** (2019) 178357.

[22] B. Wang, W. Huang, Z. Ji, Z. Wang, Y. Sun, and L. Weng, Trans. Nonferrous Met. Soc. China. **23** (2013) 1633.

[23] Q. Li, W. H. Zhang, Y. J. Yu, F. S. Liu, W. Q. Ao, and J. L. Yan, J. Alloys Compd. **487** (2009) 116.

[24] L. Zeng, P. Qin, L. Nong, J. Zhang, and J. Liao, J. Alloys Compd. **437** (2007) 84.

[25] L. Jingqi, L. Wenjun, and W. Lina, J. Rare Earth. **24** (2006) 582.

[26] W. He, L. Tang, L. Yang, J. Wen, and L. Zeng, J. Alloys Compd. **491** (2010) 149.

[27] W. Kraus, and J. Nolze, Powder Diffr. **13** (1998) 256.

[28] J. Rodriguez-Carvajal, Physica B. **55** (1993) 192.

[29] H. Rietveld, J. Appl. Crystallogr. **2** (1969) 65.

[30] H. Rietveld, Acta Crystallogr. **22** (1967) 151.

[31] L. Bessais, and C. Djega-Mariadassou, Phys. Rev. B. **63** (2001) 54412

[32] L. Bessais, S. Sab, C. Djega-Mariadassou, N. H. Dan, and N. X. Phuc, Phys. Rev. B. **70** (2004) 134401

[33] G. F. Kobzenko, E. L. Martynschuk, and L. V. Moiseeva, Dopov. Akad. Nauk Ukr. RSR, Ser A (in Russ.) **A4** (1972) 374.

[34] K. A. Gschneidner Jr, F. W. Calderwood, and Jr. Calderwood, Binary Alloy Phase Diagrams, ASM International, Materials Park **OH** (1991) 1604.

[35] V. E. Terekhova, E. V. Maslava, and Y. M. Savilsky, Russ. Metall. **3** (1965) 50.

[36] A. E Ray, Acta Crystallogr. **21** (1966) 426.

[37] G. Schneider, E. T. Henig, G. Petzow, and H. H. Stadelmaier, Z. Metallkd. **78** (1987) 694.

[38] F. Faudot, M. Harmelin, J. Bigot, S. Argouin, and P. Gouerou, Thermochim. Acta. **147** (1989) 205.

[39] F. J. G. Landgraf, G. S. Schneider, V. Villas-Boas, and F. P. Missell, J. Less Common Met. **163** (1990) 209.

[40] R. Marazza, P. Riani, and G. Cacciamani, Inorg. Chim. Acta. **361** (2008) 3800.

[41] G. X Chengfu, C. G Zhengfei, M. Lei, and Z. Bo, J. Alloys Compd. **424** (2006) 128.

[42] K. H. J Buschow, and A. S. Van Der Goot, Phys. Status Solidi. **35** (1969) 515.

[43] A. Meyer, J. Less Common Met. **18** (1969) 41.

[44] V. E. Kolesnikov, V. F Trekhova, and E. M. Savitskii, Neorg. Mater. **7** (1971) 495.

[45] G. J. Zhou, Z. W. Liu, D. C. Zeng, and Z. P. Jin, Physica B. **405** (2010) 3590.

[46] A. V Morozkin, J. Alloys and Compd. **373** (2004) L3.

[47] G. Y. Huo, Z. Y. Qiao, G. H. Rao, X. L. Chen, and J. K. Liang, J. Alloys Compd. **292** (1999) L1.

[48] C. X. Liu, Y. Sun, Z. Liu, and C. Lin, J. Appl. Phys. **76** (1994) 6766.

[49] A. V. Morozkin, and Y. D. Seropegin, J. Alloys Compd. **365** (2004) 168.

[50] N. Bouchaala, M. Jemmali, T. Bartoli, K. Nouri, I. Hentech, S.Walha, L. Bessais, and A. B. Salah J. Solid State Chem. **258** (2018) 501.

[51] Y. G. Pastushenkov, K. P. Skokov, E. S. Antonova, T. I. Ivanova, and J. S. Bartolom, J. Alloys Compd. **689** (2016) 894.

[52] Y. G. Xiao, G. H. Rao, Q. Zhang, G. Y. Liu, Y. Zhang, and J. K. Liang, J. Alloys Compd. **419** (2006) 15.